The saddle-node Hopf bifurcation with global reinjection

Bernd Krauskopf and Bart E. Oldeman

Department of Engineering Mathematics, University of Bristol, Bristol BS8 1TR, UK.

E-mail: Bernd.Krauskopf@bristol.ac.uk, Bart.Oldeman@bristol.ac.uk

August 2003

Abstract. A simultaneous saddle-node and Hopf bifurcation is a basic codimension-two local bifurcation of vector fields with a phase space of dimension at least three. Its local unfoldings are now well-known and it has been found as an organizing center of the dynamics in many vector fields arising in applications.

We study this very bifurcation, but in the presence of a reinjection mechanism that causes trajectories to return to the relevant local neighbourhood in phase space. This happens in applications, for example, in a semiconductor laser subject to optical injection, where the saddle-node bifurcation takes place on an invariant circle.

We derive and study a $\mathbb{Z}_2$-symmetric planar vector field with an additional 2π periodicity as a global model for the planar vector field reduction near a saddle-node Hopf bifurcation with global reinjection. This vector field, whose phase space is a half-cylinder, is as simple as possible and acts as a model vector field for this global bifurcation.

We present two-parameter unfoldings for the different cases of the saddle-node Hopf bifurcation in the presence of global reinjection. New phenomena that we find are periodic, homoclinic and families of heteroclinic orbits that wind around the cylinder. The theoretical unfoldings are confirmed with careful numerical investigations of these global bifurcations. We demonstrate how our results can be applied to a model of a semiconductor laser with optical injection.

Submitted to: *Nonlinearity*

AMS classification scheme numbers: 37G10 37G15 34C14 34C37 34C60

1. Introduction

The basic local codimension-one bifurcations of a generic vector field are the saddle-node bifurcation, where zero is an eigenvalue, and the Hopf bifurcation, where there is a pair of purely imaginary eigenvalues. One class of local codimension-two bifurcations, which are determined entirely by conditions on the linear part of the vector field, are given by a coincidence of two codimension-one bifurcations. These are the Bogdanov-Takens bifurcation (double-zero eigenvalue), the saddle-node Hopf bifurcation and the double-Hopf bifurcation. The unfoldings of these local bifurcations are now well known and can be found in any text book on bifurcation theory, for example, in [7, 16, 23].

In this paper we are concerned with the saddle-node Hopf (SNH) bifurcation, which is characterized by one zero eigenvalue and one pair of purely imaginary eigenvalues. The center manifold of this bifurcation is three-dimensional and it is known that very complicated dynamics can be found in a local neighbourhood of the singularity. Due to the S^1-symmetry of the normal form of the Hopf bifurcation, the local Poincaré map can be approximated up to any order by the time-1 map of a $\mathbb{Z}_2$-symmetric planar vector field. This reduces the saddle-node Hopf bifurcation to a saddle-node pitchfork (SNP) bifurcation, a codimension-two bifurcation in the class of reflectionally symmetric planar vector fields.

The codimension-two unfoldings in this class were derived and studied by Guckenheimer [15] and by Gavrilov [12, 13, 14], which is why the SNH bifurcation is also called the Guckenheimer-Gavrilov bifurcation. The normal one finds in text books, such as [7, 16, 23], is given as the two-jet

$$\begin{aligned} \dot{x} &= \mu_1 x - axy \\ \dot{z} &= \mu_2 + sx^2 - y^2. \end{aligned} \tag{1}$$

This normal form is sufficient to distinguish the six different cases of unfoldings, which are given by the genericity conditions $a \neq 0$ and $a \neq 1$ and the sign of s (which can be scaled to ± 1). However, the two-jet does not unfold all of these cases. In two cases the vector field features a family of periodic orbits (as it is Hamiltonian) for certain choices of the unfolding parameters. This can be resolved by considering terms of order three.

In [19] codimension-three unfoldings of reflectionally symmetric vector fields were considered. This required the derivation and study of the four-jet of the normal form

$$\begin{aligned} \dot{x} &= \mu_1 x - axy - x^3 \\ \dot{y} &= \mu_2 + \mu_3 x^2 - y^2 + bx^4 \,, \end{aligned} \tag{2}$$

which is valid in a neighbourhood of the singularity $(x, y, \mu_1, \mu_2, \mu_3) = (0, 0, 0, 0, 0)$. The extra codimension comes from the fact that the coefficient s in (1) is now the unfolding parameter μ_3 that is allowed to vary through 0. Among the extra genericity conditions one finds $a \neq 0, \frac{1}{2}, 1$; see [19] for details. This fourth-order normal form also provided a better understanding of the codimension-two unfoldings in that it includes an extra saddle point in a local neighbourhood of the singularity. In other words, the four-jet (2)

makes a statement in a larger neighbourhood of the respective SNP point than the two-jet, which is an advantage when one wants to identify dynamics near a SNH bifurcation (or an SNP bifurcation) in a vector field arising in an application.

Indeed the SNH bifurcation was identified in many applications as an organizing center of the dynamics, for example, in a model of travelling waves of calcium in pancreatic acinar cells [27], the Lorenz-84 model [26], in the Taylor-Couette flow [25] in a binary fluid convection [18] in rotating convection [24], and in a laser with optical injection [33, 20, 32, 22], the motivating example for the work presented here. We remark that in these applications one encounters the most interesting case of the SNH bifurcation, namely that featuring a perturbed invariant sphere ($s < 0$ and $a < 0$ in (1), which is case III in the notation of [16]), near which Shilnikov orbits are known to exist in a full three-dimensional unfolding that breaks the S^1-symmetry of the normal form [2, 11].

For the injection laser introduced in section 4 any orbit leaving a small neighbourhood in phase space near the SNH point will return after a 2π phase jump of the laser light to the same neighbourhood. This is reflected in the laser equations by a 2π-periodic variable; see section 4. The 2π-periodicity provides a reinjection mechanism that is responsible for new dynamics, such as periodic orbits that combine phase jumps with dynamics near the SNH point; see, [32, 28, 34, 33]. More generally, reinjection is present when the SNH bifurcation takes place 'on a periodic orbit', meaning that the unstable part of the one-dimensional center manifold of the saddle-node bifurcation returns (close) to the saddle-node Hopf point, as is sketched in figure 1.

A general situation in which a SNH bifurcation takes place on a periodic orbit is that of a weak resonance of a periodic orbit of a vector field. It is known that the boundary of the associated resonance tongue of a $p : q$ resonance where $q > 4$ is formed by a saddle-node bifurcation of a periodic orbit (of winding number $p : q$) that takes place on an invariant circle [7, 16, 23]. Furthermore, SNH bifurcations generally occur on the boundary of the resonance tongue, which is formed by a codimension-one saddle-node bifurcation of periodic orbits. In other words, modulo the $\mathbb{Z}_q$ rotational symmetry that is inherent in this situation, one finds a SNH bifurcation with global reinjection. For a numerical study of a SNH bifurcation with global reinjection in a 1:5 resonance tongue see [31].

We remark that the global reinjection we consider is not due to the S^1-symmetry associated with the Hopf normal form. Indeed, in the planar reflectionally symmetric vector field approximation, we are dealing with a SNP bifurcation with global reinjection.

In this paper we study this generic codimension-two bifurcation, the saddle-node pitchfork bifurcation with global reinjection, in the general setting of bifurcation theory. (How one can translate our results back to the case of a SNH bifurcation with global reinjection of the original vector field is briefly discussed in section 5.) We consider a simple planar reflectionally symmetric vector field with an additional translational symmetry, which we assume to be translation over 2π. Specifically, we choose to work

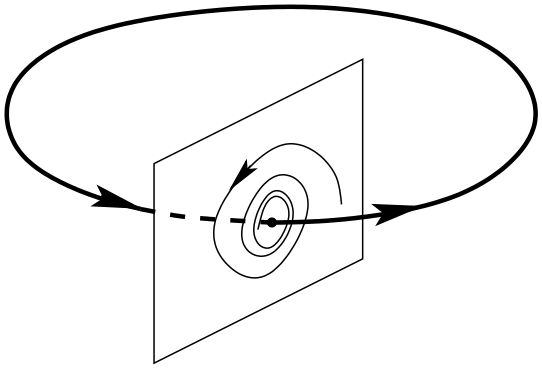

Figure 1. Sketch of the SNH bifurcation with reinjection.

with the vector field

$$\begin{aligned} \dot{x} &= \nu_1 x - a \sin\varphi x - x^3 \\ \dot{\varphi} &= \nu_2 + s x^2 + 2\cos\varphi + c x^4 \end{aligned} \tag{3}$$

because it is as simple as possible and yet feature a SNP bifurcation with global reinjection with a sufficient number of higher order coefficients. In this sense it acts as a global vector field model for the SNP bifurcation with global reinjection. Although a different choice of model vector field would not be topologically equivalent, we believe that the model we present represents a good balance between including a wide range of possible dynamics while being simple enough to allow for some analysis. In particular, in a neighbourhood of the SNP singularities $(x, \varphi, \nu_1, \nu_2) = (0, 0, 0, -2)$ and $(x, \phi, \nu_1, \nu_2) = (0, \pi, 0, 2)$ we retrieve the full four-jet.

By identifying the boundaries of a fundamental domain of the symmetry, the model equation is revealed as a vector field on a half-cylinder. (The other half is the counterpart under the $\mathbb{Z}_2$-symmetry.) An excursion around the cylinder corresponds to global reinjection. In the plane of unfolding parameters we find two SNP points on the invariant circle $\{x = 0\}$, one at 0 and one at π. When expanding out sine and cosine by their Taylor series at these points we recover the four-jet of the normal form (2). What is more, the two SNP points differ in exactly the sign of the coefficient b. In other words, in the (ν_1, ν_2)-plane of (3) we recover the same bifurcations that were found in the presented codimension-three unfoldings in [19]. (Note that the codimension-three study in [19] is concerned with a single SNP singularity, while we are dealing here with *two different* SNP singularities, one on each side of the cylinder.) This is a huge advantage and allows us to start our investigation of the SNP bifurcation with global reinjection from a firm skeleton of local bifurcations. For consistency we follow the notation in [19] as much as possible. The next and important step is to find all dynamics and bifurcations that are caused by the reinjection mechanism, that is, include an excursion around the cylinder. We present the simplest, consistent unfoldings and present numerical evidence that they are correct. This is done by the numerical continuation of periodic, homoclinic and heteroclinic orbits with the continuation package AUTO [10], in combination with

a study of selected phase portraits with software DSTool [1].

The paper is organized as follows. In section 2 we discuss the model vector field and perform an algebraic analysis to obtain as much information as possible for all parameter values. Subsequently, section 3 discusses four cases A–D of bifurcation diagrams, which are presented as qualitative sketches as well as numerical bifurcation diagrams. In section 4 we show how the most complicated case D organised the behaviour in a model of a laser with optical injection. Finally, we discuss the interpretation of our results and draw some conclusions in section 5.

2. Local bifurcation analysis

In this section we present a local bifurcation analysis of system (3) and show how it can be reduced near the SNP points to the generic four-jet that is given by equation (2). This reduction provides evidence that we can find the same bifurcations in system (3) as were found in the unfoldings of [19]. The investigation of the local bifurcations in the (ν_1, ν_2)-plane (and all other parameters remain fixed) provides the framework for the global analysis presented in the next section. We also investigate some of the symmetries that are involved.

Lemma 1. *The following local bifurcations are part of the bifurcation set of (3):*

(i) Two lines of saddle-node bifurcations S_0 on the invariant circle (that is, for $x = 0$), given by $\nu_2 = \pm 2$;

(ii) an ellipse of pitchfork bifurcations P given by

$$\left(\frac{\nu_1}{a}\right)^2 + \left(\frac{\nu_2}{2}\right)^2 = 1\,;$$

(iii) two curves of saddle-node bifurcations S off the invariant circle; if $c = 0$ then these curves are straight lines given by

$$\nu_2 = \pm\sqrt{4 + (as)^2} - s\nu_1\,;$$

for all values of c, their endpoints on P are given by

$$(\nu_1, \nu_2) = \pm\left(\frac{a^2 s}{\sqrt{4 + (as)^2}}, \frac{4}{\sqrt{4 + (as)^2}}\right). \tag{4}$$

(iv) two SNP points at the intersection points $(\nu_1, \nu_2) = (0, \pm 2)$ of S_0 and P;

(v) a Bogdanov-Takens bifurcation on S; if $c = 0$ then it is given by

$$\nu_1 = \frac{(1-a)as}{\sqrt{4 + (as)^2}}. \tag{5}$$

Proof. Solving equation (3) for equilibria gives the following solutions:

$$(x, \varphi) = (0, \arccos(-\nu_2/2)), \qquad -2 \le \nu_2 \le 2 \tag{6}$$

$$(x, \varphi) = (0, -\arccos(-\nu_2/2)), \qquad -2 \le \nu_2 \le 2 \tag{7}$$

$$(x, \varphi) = (\hat{x}, \hat{\varphi}), \text{ where } \sin\hat{\varphi} = \frac{\nu_1 - \hat{x}^2}{a} \text{ and } \left(\frac{\nu_1 - \hat{x}^2}{a}\right)^2 + \left(\frac{\nu_2 + s\hat{x}^2 + c\hat{x}^4}{2}\right)^2 = 1, \tag{8}$$

where we have $2\cos\phi = -\nu_2$ for solutions (6) and (7). It follows that there are saddle-node bifurcations of equilibria for $x = 0$ along the lines $\nu_2 = \pm 2$. Moreover, a pitchfork bifurcation that affects the two types of equilibria (on and off the invariant circle) exists where these two equilibria coincide, that is, along the ellipse

$$\left(\frac{\nu_1}{a}\right)^2 + \left(\frac{\nu_2}{2}\right)^2 = 1\,.$$

The Jacobian matrix is given by

$$\begin{pmatrix} \nu_1 - a\sin\varphi - 3x^2 & -ax\cos\varphi \\ 2sx + 4cx^3 & -2\sin\varphi \end{pmatrix} \tag{9}$$

which at $(x,\varphi) = (0, \pm\arccos(-\nu_2/2))$ reduces to

$$\begin{pmatrix} \nu_1 & 0 \\ 0 & 0 \end{pmatrix} \pm \begin{pmatrix} a\sqrt{1-\frac{\nu_2^2}{4}} & 0 \\ 0 & 2\sqrt{1-\frac{\nu_2^2}{4}} \end{pmatrix} \tag{10}$$

so that for $\nu_1 \neq 0$ and $\nu_2 = \pm 2$ generic saddle-node bifurcations S_0 occur along the invariant circle. At the equilibria defined by (8) the Jacobian matrix equals

$$\begin{pmatrix} -2x^2 & -ax\cos\varphi \\ 2sx + 4cx^3 & -2\sin\varphi \end{pmatrix} \tag{11}$$

where $\nu_1 - a\sin\varphi - x^2 = 0$, giving a pitchfork bifurcation P for $x = 0$. SNP bifurcations occur at the tangency points $(\nu_1,\nu_2) = (0,\pm 2)$ of S_0 and P. Their normal form is considered in Lemma 2.

A saddle-node bifurcation S involving the equilibria off the invariant circle (that is, those with $x \neq 0$) given in (8) occurs when the determinant of the Jacobian matrix in (11) is zero, that is, if

$$4x^2\sin\varphi + (2sx + 4cx^3)ax\cos\varphi = 0,$$

$$2\sin\varphi + (s + 2cx^2)a\cos\varphi = 0.$$

It is not possible to solve this equation analytically in a straightforward manner if $c \neq 0$. However, the endpoints of the saddle-node bifurcation curves S on the pitchfork bifurcation curve P can be determined analytically, because then we can consider the limiting point where $x = 0$. Hence, $2\sin\varphi + as\cos\varphi = 0$, which, combined with the solution equations (6/7) and (8) gives

$$(\nu_1,\nu_2) = \pm\left(\frac{a^2 s}{\sqrt{4+(as)^2}}, \frac{4}{\sqrt{4+(as)^2}}\right).$$

For $c = 0$ it is possible to analytically determine the full saddle-node bifurcation curves S as the straight lines

$$\nu_2 = \pm\sqrt{4+(as)^2} - s\nu_1\,.$$

At a Bogdanov-Takens bifurcation the trace of the Jacobian matrix must be zero, hence $x^2 + \sin\varphi = 0$. This gives the location of the Bogdanov-Takens bifurcation as

$$\nu_1 = \frac{(1-a)as}{\sqrt{4+(as)^2}}$$

on one of the lines S (which one depends on the sign of a).

□

We now show that equation (3) can be reduced near the SNP points to a generic four-jet.

Lemma 2. *System (3) has two SNP points at* $(x,\varphi,\nu_1,\nu_2) = (0,0,0,2)$ *and* $(x,\varphi,\nu_1,\nu_2) = (0,\pi,0,-2)$*, that is, on the invariant circle* $\{x=0\}$*. In a neighbourhood of these points (3) can be transformed to the four-jet normal form (2) by suitable coordinate transformations, where* $(\mu_1,\mu_2,\mu_3,a,b) = (\nu_1, 2+\nu_2, \mu_3, a, c+\mu_3^2/12)$ *and* $(\mu_1,\mu_2,\mu_3,a,b) = (\nu_1, -2-\nu_2, -\mu_3, a, -c+\mu_3^2/12)$*, respectively.*

Proof. Taylor expanding the trigonometric terms in (3) (up to order four) around the first SNP point $(x,\varphi,\nu_1,\nu_2) = (0,0,0,2)$ gives

$$\begin{aligned}
\dot{x} &= \nu_1 x - a\varphi x - ax\frac{\varphi^3}{6} - x^3 + O(|(x,\varphi)|^5) \\
\dot{\varphi} &= \nu_2 + 2 + sx^2 - \varphi^2 + \frac{\varphi^4}{12} + cx^4 + O(|(x,\varphi)|^5)\,.
\end{aligned} \tag{12}$$

Hence, we can set $(\mu_1,\mu_2,\mu_3) = (\nu_1, 2+\nu_2, \mu_3)$ in the vicinity of the SNP point $(\nu_1,\nu_2) = (0,2)$. We now bring equation (12) into the form (2) by means of coordinate transformations, where we follow the procedure in [19]. The coordinate transformation

$$\begin{aligned}
u &= x + Ax^3 + Bx\varphi^2 \\
v &= \varphi + Cx^2\varphi + D\varphi^3
\end{aligned} \tag{13}$$

gives

$$\begin{aligned}
\dot{u} &= \mu_1 u - (a - 2\mu_2 B)uv + (-1 + 2\mu_1 A)u^3 \\
&\quad + (aC - 2aA + 2\mu_3 B - 2\mu_2 AB - 2\mu_2 BC)u^3 v \\
&\quad + (-\frac{a}{6} + aD - 2B - 2\mu_2 BD - 2\mu_2 B^2)uv^3 + O(|(u,v)|^5) \\
\dot{v} &= \mu_2 + (\mu_3 + \mu_2 C)u^2 + (-1 + 3\mu_2 D)v^2 + (2C\mu_1)u^2 v \\
&\quad + (c - 2\mu_2 AC + C\mu_3 - 2\mu_3 A)u^4 \\
&\quad + ((1-2a)C - 2\mu_2 BC - 6\mu_2 CD - 2\mu_3 B + 3\mu_3 D)u^2 v^2 \\
&\quad + (\frac{1}{12} - D - 6\mu_2 D^2)v^4 + O(|(u,v)|^5)
\end{aligned} \tag{14}$$

where μ_1 and μ_2 are small. We now compare (14) with (2), neglecting terms in μ_1 and μ_2. This yields the set of equations

$$\begin{aligned} a(C-2A)+2\mu_3 B &= 0 \\ -\frac{a}{6}+aD-2B &= 0 \\ c+(C-2A)\mu_3 &= b \\ ((1-2a)C-2\mu_3 B+3\mu_3 D &= 0 \\ \frac{1}{12}-D &= 0 \end{aligned} \tag{15}$$

Eliminating A, B, C, and D gives $c+\mu_3^2/12=b$.

To obtain the four-jet normal form near the second SNP point $(x,\varphi,\nu_1,\nu_2)=(0,\pi,0,-2)$, we use the substitution $\varphi\mapsto\pi-\varphi$, yielding

$$\begin{aligned} \dot{x} &= \nu_1 x - a\sin\varphi x - x^3 \\ \dot{\varphi} &= -\nu_2 - sx^2 + 2\cos\varphi - cx^4. \end{aligned} \tag{16}$$

With sign changes of ν_2, s and c, the result follows.

□

Note that the above proof reveals a symmetry in equation (3): the substitution

$$(\varphi,\nu_2,s,c)\mapsto(\pi-\varphi,-\nu_2,-s,-c) \tag{17}$$

leaves the system invariant, so that one can restrict to the case $c\geq 0$.

3. Global bifurcation diagrams

The above analysis gives a lot of information about the basic structure of the bifurcation diagrams. In every instance of a bifurcation diagram in the (ν_1,ν_2)-plane we find two SNP points at $(x,\varphi,\nu_1,\nu_2)=(0,0,0,2)$ and $(x,\varphi,\nu_1,\nu_2)=(0,\pi,0,-2)$ that differ in sign of μ_3 in their four-jet normal form (2). As a consequence, these two SNP points are connected in the (ν_1,ν_2)-plane exactly as they are connected on a sphere around the codimension-three unfoldings in [19]. In other words, the respective bifurcation diagrams from [19] act as the framework for the unfoldings of the SNH bifurcation with global reinjection.

The goal is now to 'complete' this local framework by taking into account the global reinjection. We follow the notation of [19] and first consider the three basic cases A, B and C where (2) provides the connection between the respective cases + and − (for the sign of μ_3) of the SNP bifurcation. A sketch of the (a,c)-plane of (3) with the regions A, B, C is shown in figure 3. Further subcases, which differ in some small details, have been identified in [19]. However, to keep the discussion focused we only present one representative case each for A, B and C with global reinjection. Below we will also consider an even more complicated case D, which is not fully unfolded in (2), but is relevant to the laser with injection in section 4. The boundary between case A and case

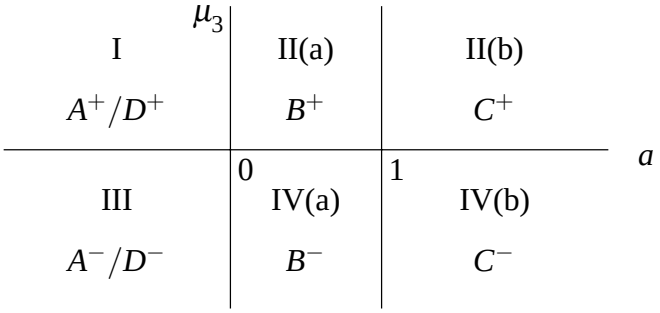

Figure 2. Regions corresponding to different qualitative bifurcation in the (a, μ_3)-plane of (2); the Roman numerals are the notation from [16].

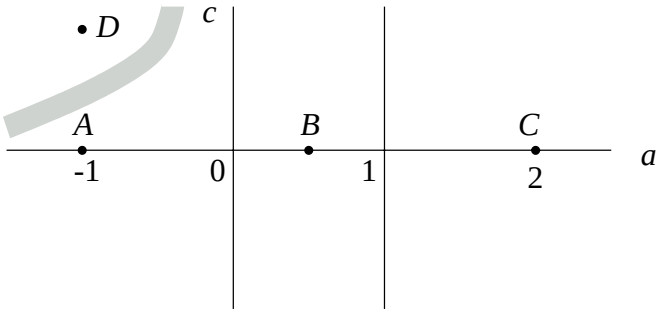

Figure 3. Regions corresponding to different qualitative bifurcation behaviour in the (a, c) plane for $s < 0$. The dots correspond to the particular cases we looked at numerically.

D is not a single curve as it involves quite a number of codimension-three bifurcations. It is suggested in figure 3 by the grey boundary.

In what follows we present for each case A to D, containing two SNP bifurcation with global reinjection, a topological bifurcation diagram followed by a numerical bifurcation diagram featuring relevant enlargements. Our approach has been to construct a consistent minimal bifurcation diagram for each case by starting from the respective case in [19] of two local SNP bifurcations and consider what happens if the dynamics takes place on a cylinder, providing the global reinjection. This is highlighted in the figures in this paper as follows. Any bifurcation curves that are plotted as normal curves in the bifurcation diagrams already appear without reinjection. On the other hand, any curve that is shown in boldface is of a bifurcation that is due to global reinjection. Examples of this are bifurcations of periodic orbits that go around the cylinder. The bifurcation diagrams are surrounded by sketches of the dynamics on the half-cylinder. (Top and bottom of each panel need to be identified.) All phase portraits are numbered in a consistent manner throughout the entire paper. To aid the interpretation of the bifurcation diagrams that follow, figure 4 shows sketches of (and introduces the notation for) the different kinds of homoclinic and heteroclinic orbits

that we encounter.

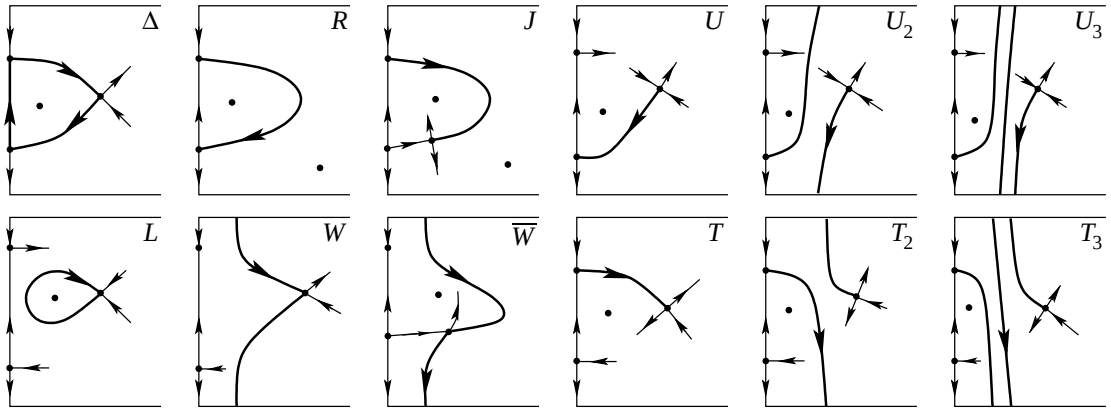

Figure 4. Phase portraits of heteroclinic and homoclinic bifurcations.

The consistent minimal bifurcation diagrams were also verified by computing phase portraits with the package DsTool[1] and by computing bifurcation curves with AUTO/HomCont[4, 5, 10]. The solid dots in figure 3 indicate the values of a and c that we used in our numerical investigations. Further we choose $s = -1$. (The case $s = 1$ can be inferred by the symmetry (17). In particular, we computed homoclinic and heteroclinic orbits by using either a homotopy method or by starting the continuation from a periodic orbit of large period. For a homoclinic or heteroclinic orbit that winds around the cylinder we worked in the covering space $\mathbb{R}^2$ and found and followed the corresponding heteroclinic orbit. The different homoclinic and heteroclinic orbits in the system are shown as DsTool plots in figure 5, where the relevant parameter values were found with AUTO/HomCont; compare figure 4.

3.1. Case A

The bifurcation diagram for case A is sketched in figure 6. The framework of the bifurcation diagram is given by the saddle-node bifurcation lines S_0, the pitchfork ellipse P , the saddle-node bifurcation curves S, and the bifurcation curves R and H emanating from the SNP point $A-$. The latter curves interact with P and S in exactly the way found in [19]. The curve R bifurcates into a heteroclinic orbit J and a homoclinic loop L at the pitchfork bifurcation P. The curve J terminates at the saddle-node bifurcation S, whereas L and H terminate at S in a Bogdanov-Takens bifurcation.

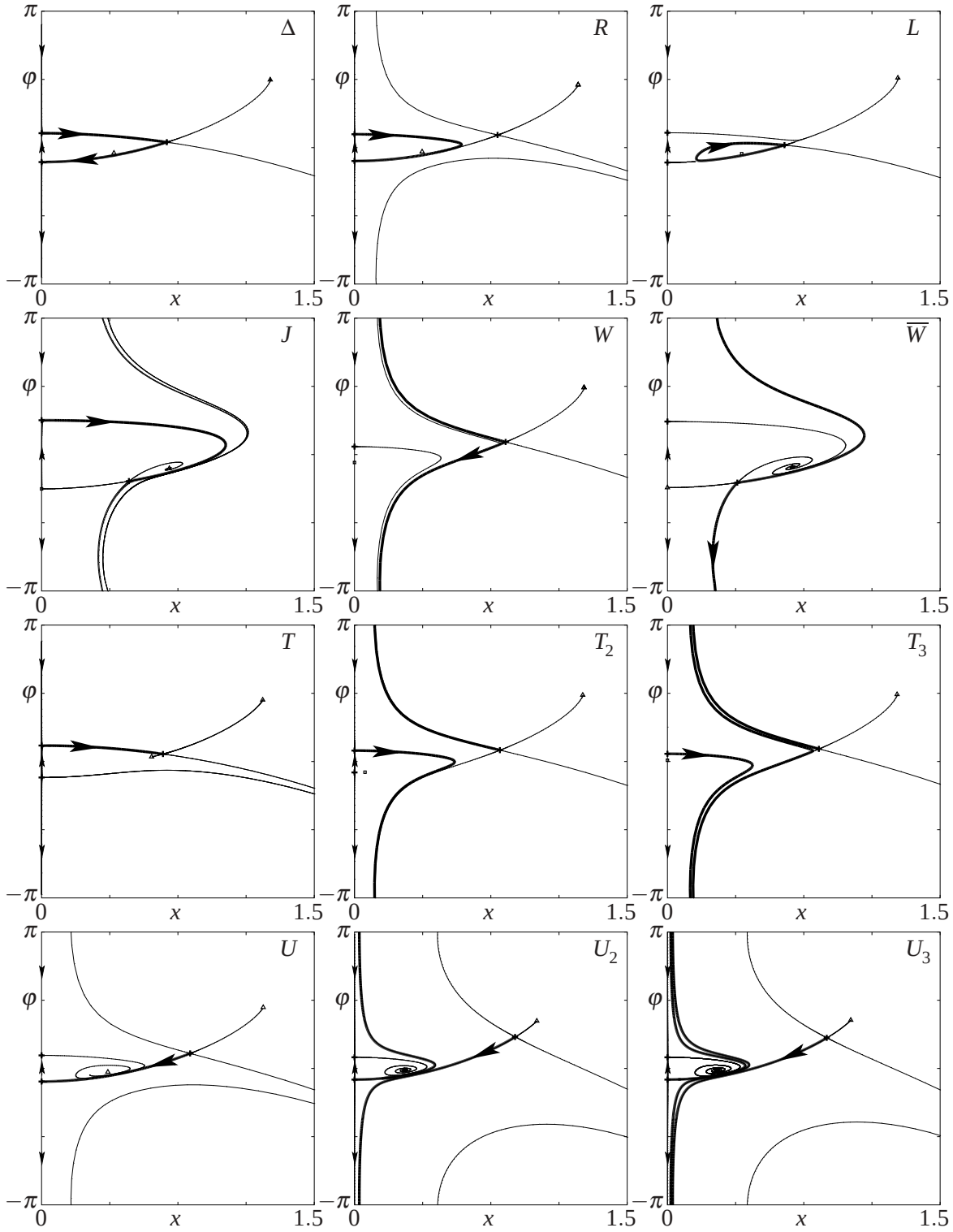

Figure 5. Numerical phase portraits of the heteroclinic and homoclinic bifurcations in figure 4. Here $s = -1$ and $a = -1$; for all other parameter values see table 1.

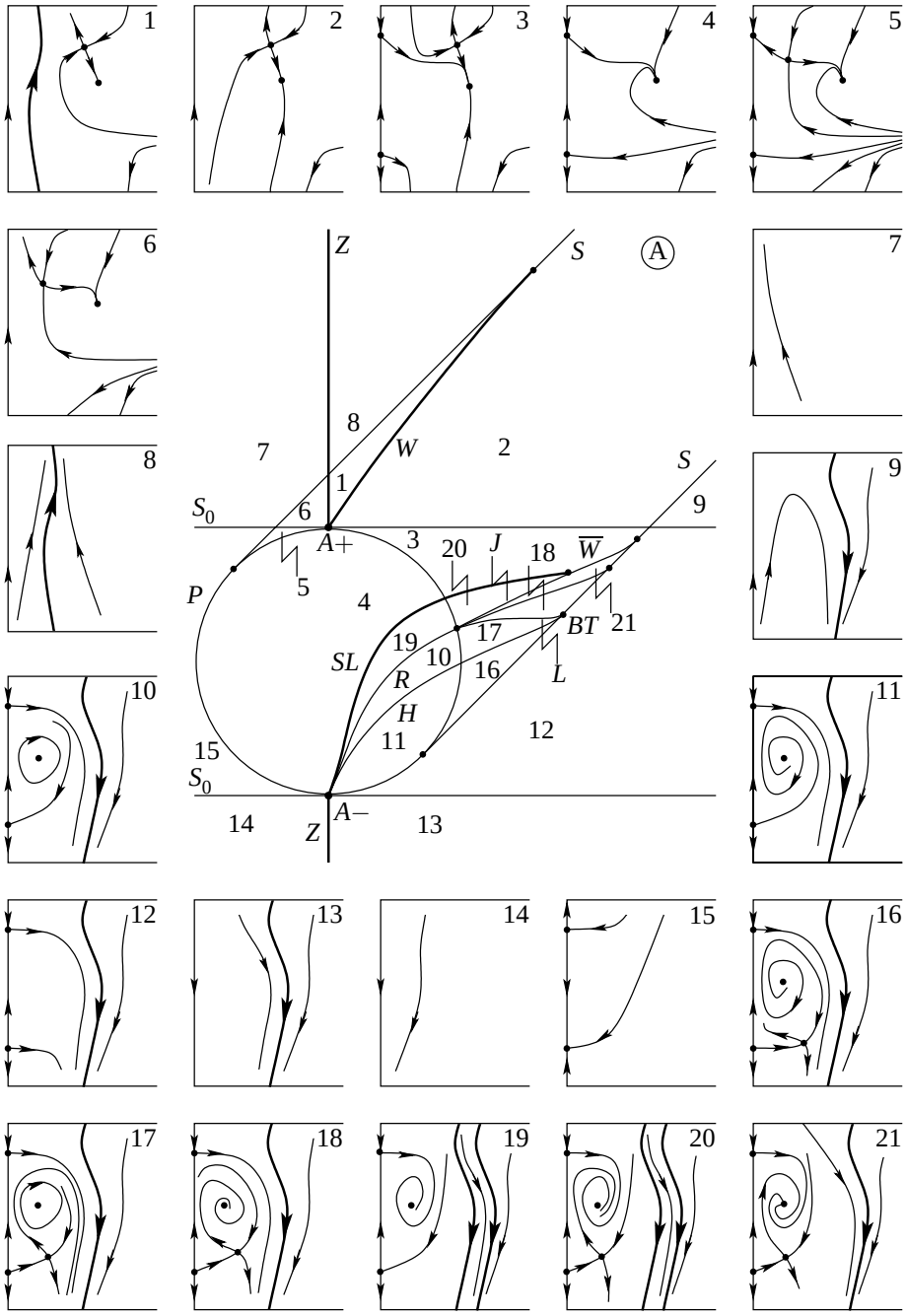

Figure 6. Qualitative bifurcation diagram for case A.

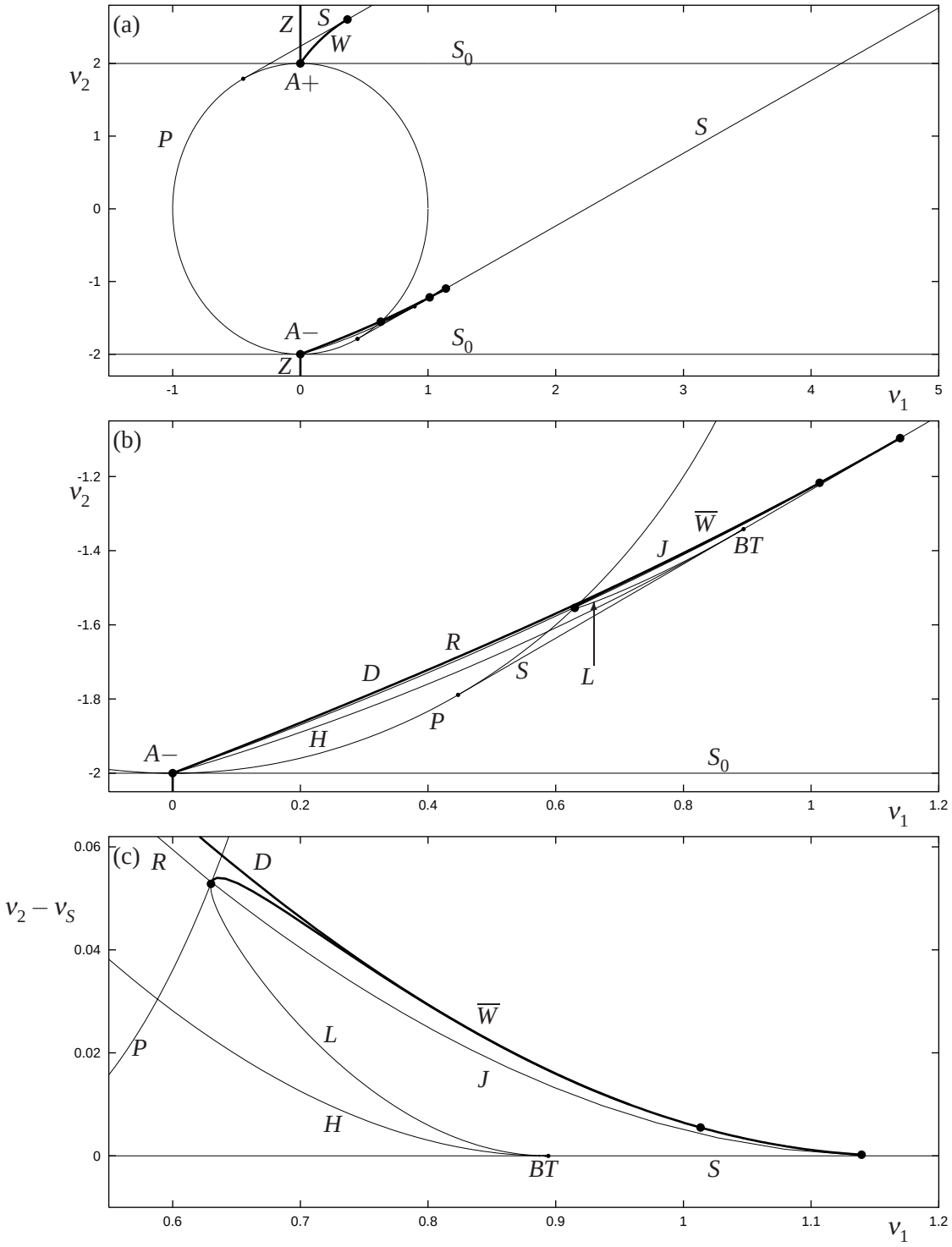

Figure 7. Numerical overview of case A (a), an enlargement of the neighbourhood of $A-$ (b) and a plot relative to the curve S in the neighbourhood of $\overline{W}$ (c). Here $s = -1$, $a = -1$ and $c = 0$.

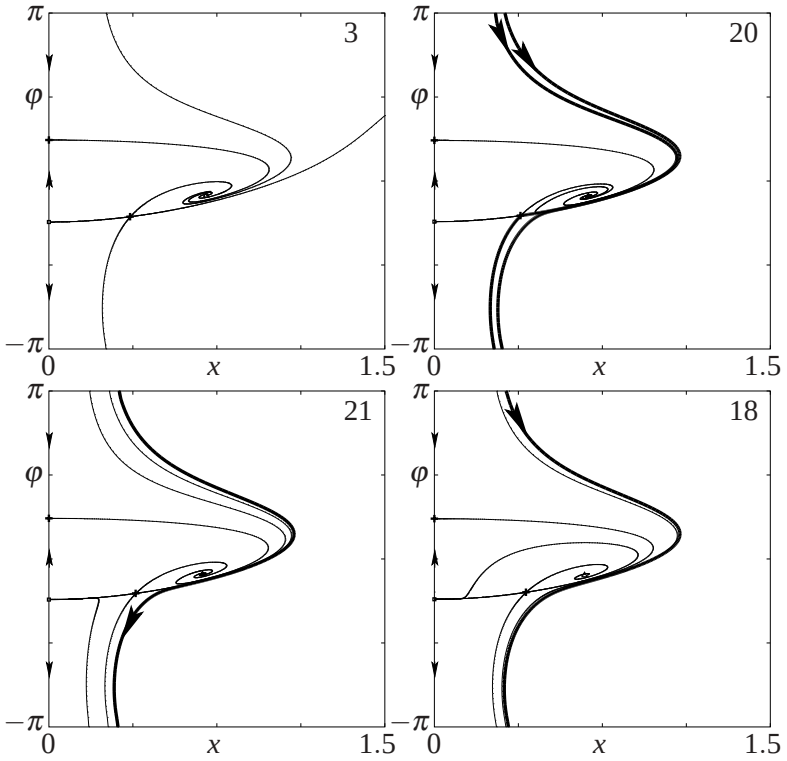

Figure 8. Numerical phase portraits corresponding to the bifurcation diagram in figure 6. Here $s = -1$ and $a = -1$; for all other parameter values see table 1.

However, when considering this scenario of bifurcation of the cylinder, effectively 'switching on' global reinjection, then one realizes that further bifurcations must take place to make the overall bifurcation diagram consistent. In this, and in fact all other cases, we find a curve Z where a periodic orbit that goes around the cylinder bifurcates from the trivial periodic orbit, the invariant circle $\{x = 0\}$. Near the point $A+$, this global periodic orbit exists in regions 1 and 8, and then bifurcates in the homoclinic bifurcation W, which is an example of a homoclinic orbit around the cylinder; see also Figures 4 and 5. Above the point where W ends on S (a non-central saddle-node homoclinic bifurcation[6]) the saddle-node bifurcation along S takes place on the global periodic orbit.

Near the point $A-$ we find that the intersection point of R and P gives rise to another homoclinic bifurcation around the cylinder, $\overline{W}$. Furthermore, the heteroclinic cycle around the cylinder made up of R and a part of the invariant circle is a repelling object, while all orbits move towards smaller values of x if x is sufficiently large. As

a result, a repelling periodic orbit around the cylinder is born along R, which coexists with an attracting periodic orbit around the cylinder in regions 19 and 20. Both periodic orbits disappear in the curve SL of saddle-node bifurcation of periodic orbits around the cylinder. This curve starts at $A-$ and ends in a point on $\overline{W}$, where the saddle quantity of the saddle is neutral. Above this point the saddle-node bifurcation again takes place on the periodic orbit around the cylinder.

The numerical plots in figure 7 were computed for $a = -1$, $c = 0$ and $s = -1$ and confirm the topological sketch in figure 6 described above. Panel (a) is an overview and panel (b) is an enlargement illustrating the scenario of bifurcations near $A-$. Finally, panel (c) is a further enlargement where all curves are plotted *relative* to the curve S, which now appears as the line $\nu_2 - \nu_S = 0$. Numerically it looks as if the heteroclinic bifurcation curve J and the homoclinic curve $\overline{W}$ end at the same point on the curve S, even though this is not possible for topological reasons.

Figure 8 gives additional numerical evidence for the existence of the curve SL. Each panel corresponds to a phase portrait in the transition from region 3 to region 18 of the bifurcation diagram in figure 6. When SL is crossed, we see in region 20 the appearance of two periodic orbits that wind around the cylinder. The unstable of these two limit cycles disappears in the homoclinic bifurcation $\overline{W}$, leaving only the stable periodic orbit in region 21. Finally, the heteroclinic bifurcation curve J results in a change of the basin of attraction of the periodic orbit.

3.2. Case B

The bifurcation diagram for case B is sketched in figure 9, with numerical plots in figure 10 that were computed for $a = 0.5$, $c = 0$, $s = -1$. Its framework is formed by the saddle-node bifurcation lines S_0, the pitchfork ellipse P, the saddle-node bifurcation curves S, and the bifurcation curves H and L emanating from the SNP point $B+$ and ending at a Bogdanov-Takens bifurcation on S.

The extra bifurcation curves due to reinjection are the curves Z, W starting at $B+$ and ending on the upper branch of S, and $\overline{W}$ starting at $B-$ and ending on the lower branch of S. The overall consistent bifurcation diagram is quite a lot simpler than in case A. This is confirmed by the overview in figure 10 (a) and the enlargements near $B-$ and $B+$ in figure 10 (b) and (c).

3.3. Case C

The bifurcation diagram for case C is very similar to that of case B. It is sketched in figure 11, with numerical plots in figure 12 that were computed for $a = 2$, $c = 0$, $s = -1$. The difference is that the Bogdanov-Takens bifurcation has 'flipped side': the bifurcation curves H and L, emanating from the SNP point $C+$ and ending at a Bogdanov-Takens bifurcation on S, changed order, leading to an attracting periodic orbit in region 32. As a result, we also see the appearance of a heteroclinic curve U bounding the small region 33.

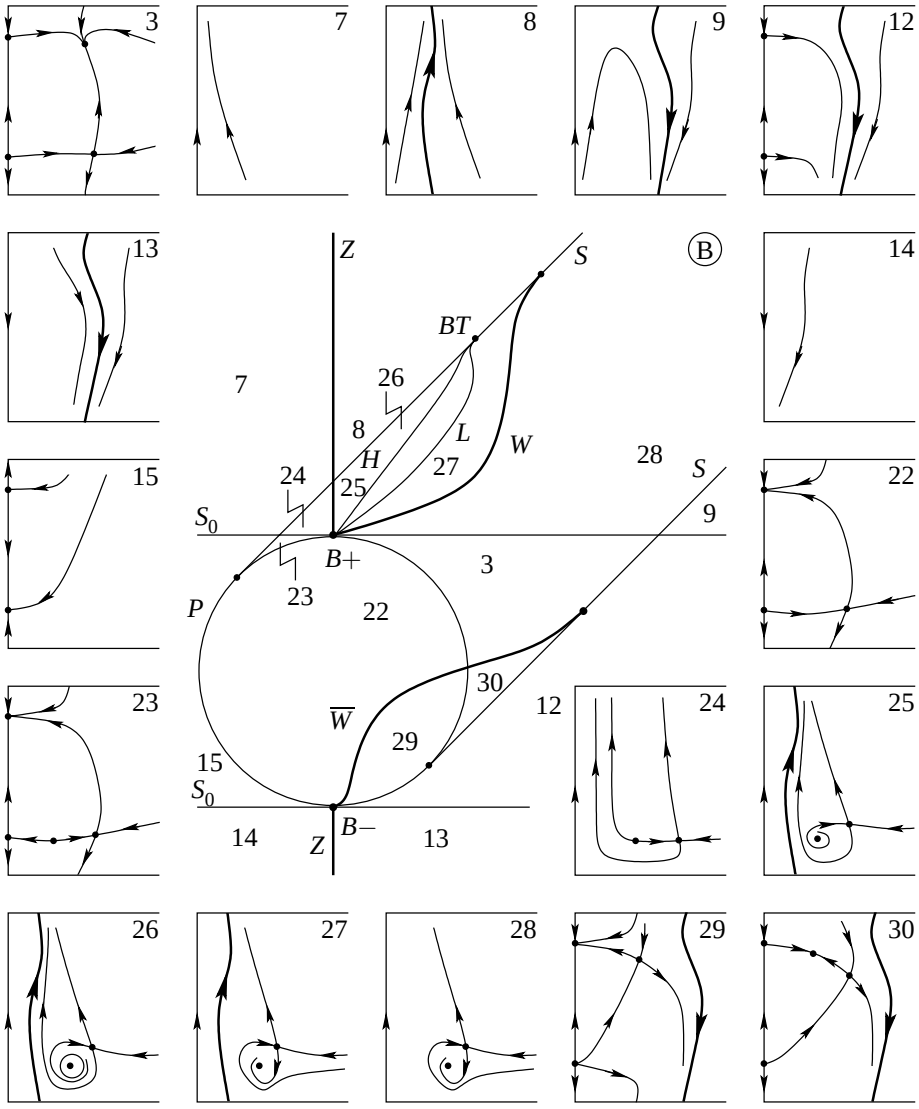

Figure 9. Qualitative bifurcation diagram for case B.

The extra bifurcation curves due to reinjection are again Z, W and $\overline{W}$. Their topological positions are just as for case B. The overview in figure 12 (a) and the enlargements near $C+$ and $C-$ in figure 12 (b) and (c) confirm the topological sketch, including the existence of the curve U.

3.4. Case D

The bifurcation diagram for case D should be directly compared with that for case A. The two cases agree in a small neighbourhood around the SNP points $A+$ and $D+$, and $A-$ and $D-$, respectively, because the difference lies in the value of the higher order term coefficient c. However, case D is much more complicated already on the level of the local information (not taking reinjection into account); see [19]. Specifically, there

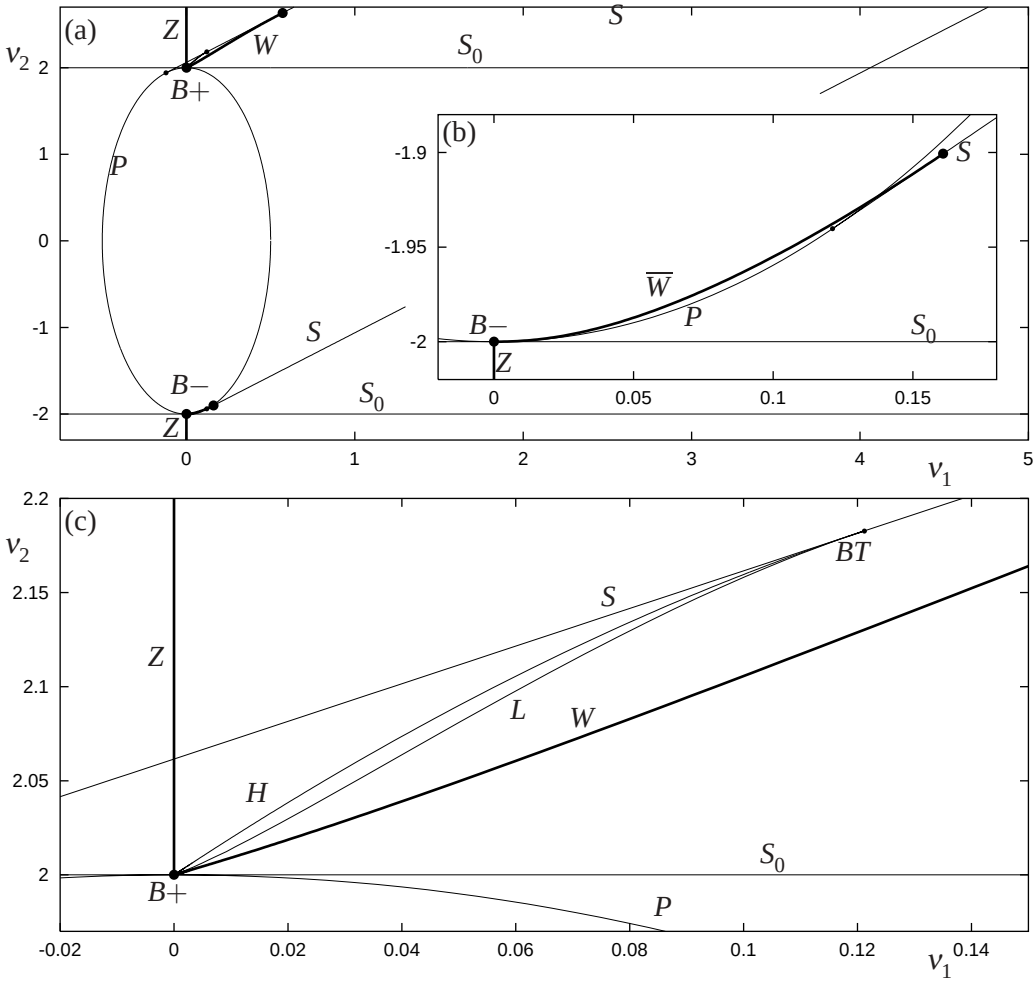

Figure 10. Numerical overview of case B (a), and enlargements of the neighbourhoods of $B-$ (b) and $B+$ (c). Here $s = -1$, $a = 0.5$ and $c = 0$.

is a codimension-two organizing center in the form of a triangular heteroclinic cycle Δ; see Figures 4 and 5. As we explain now, this leads in turn to the existence of entire cascades of extra bifurcations in the presence of reinjection.

An overview of the bifurcation diagram is shown in figure 13 with an enlargement near Δ in figure 14. The bifurcation diagram of (3) near $D+$ is topologically like that near $A+$, but near $D-$ it is quite different from that near $A-$. The curve S is no longer a straight line, because $c \neq 0$. In particular, the lower branch of S now enters the interior of the pitchfork ellipse P and also has a cusp point.

The codimension-one heteroclinic curve R ends at the codimension-two heteroclinic cycle Δ when the heteroclinic orbit hits the equilibrium off the invariant circle. This heteroclinic cycle is the limit of quite a number of curves of codimension-one homoclinic and heteroclinic orbits, because it is composed of two heteroclinic orbits and all sections of the invariant circle. Some of these orbits, namely R, L, T and U, do not make excursions around the cylinder; see Figures 4 and 5. They were already found in [19].

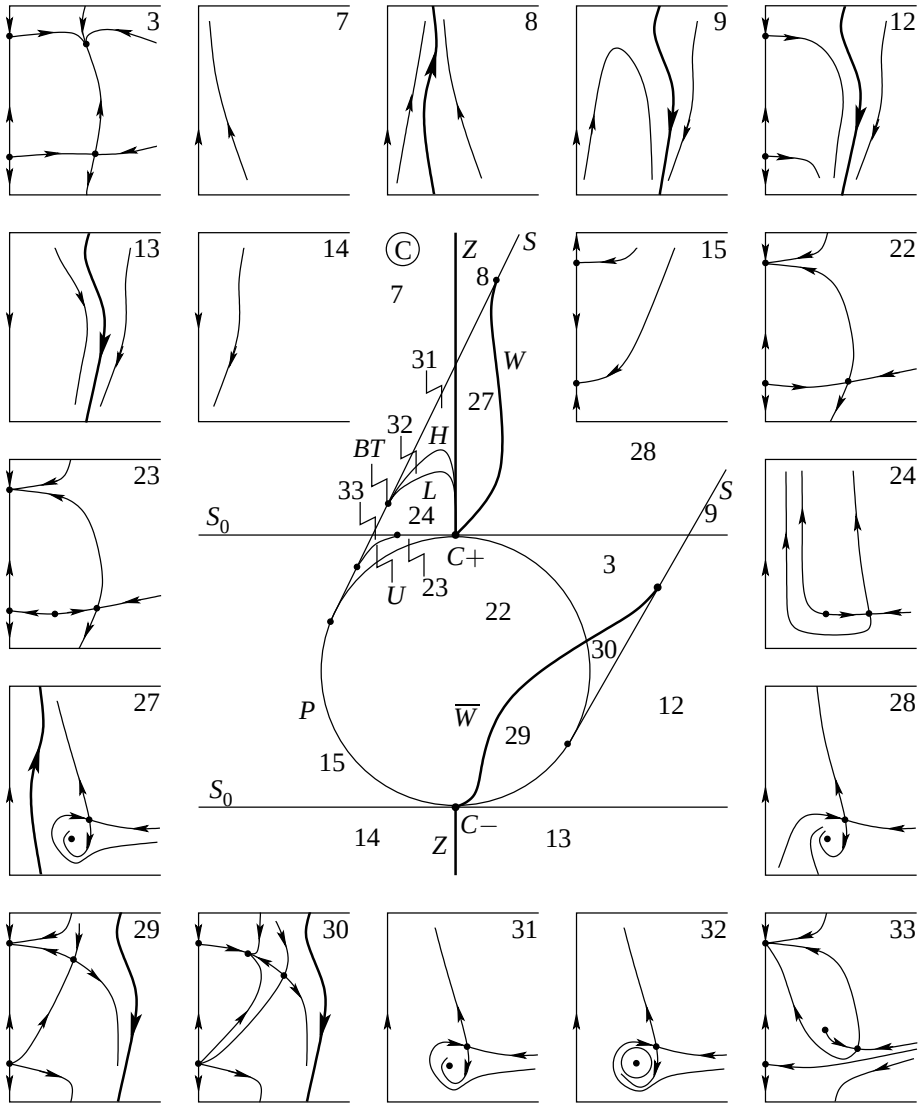

Figure 11. Qualitative bifurcation diagram for case C.

We remark that at the point Δ the four-jet normal form (2) has a family of periodic orbits, meaning that it does not unfold Δ generically. This does not appear to be the case for system (3) due to additional higher-order terms provided by the trigonometric functions in φ. In particular, the Hopf bifurcation curve misses Δ, leading to region 36 with two periodic orbits, bounded by H, L and a saddle-node of periodic orbit bifurcation curve SL.

More interesting from the point of view of this paper are curves of codimension-one homoclinic and heteroclinic orbits that include excursions around the cylinder. They are the curve W, and the sequences T_i and U_i of heteroclinic orbits that wind around the cylinder $i-1$ times before closing up; see again Figures 4 and 5.

Notice that the unstable manifold of the saddle on the invariant circle accumulates on the periodic orbit that winds around the cylinder (regions 45 and 49). This periodic

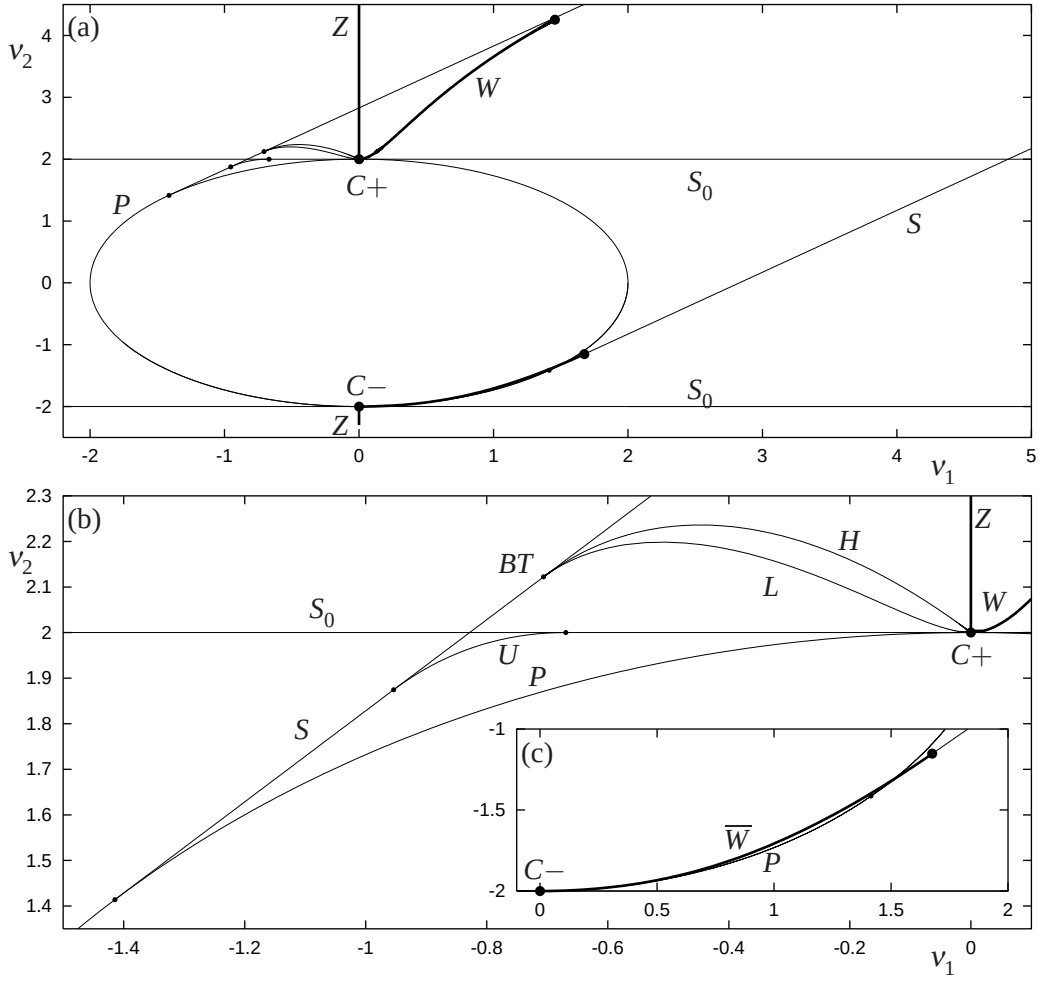

Figure 12. Numerical overview of case C (a). Enlargements of the neighbourhood of $C+$ (b) and $C-$ (c). Here $s = -1$, $a = 2$ and $c = 0$.

orbit then disappears in the homoclinic orbit W, so that it is the ω-limit set of the above unstable manifold. When the homoclinic orbit W is broken it is possible to make a heteroclinic connection between the saddle on the invariant circle and the saddle off the invariant circle. In fact, given any $i \in \mathbb{N}$ one can find a heteroclinic orbit T_i that winds $(i-1)$ times around the cylinder before connecting the two saddles at the ith turn. In other words, the curve W is the accumulation of the curves T_i as is shown in figure 14. The end points of the T_i are on the curve S_0 where the saddle on the invariant circle disappears. A similar accumulation of heteroclinic orbits U_i involves the stable manifold of the other saddle on the invariant circle. The curves U_i accumulate on the curve SL of saddle-node bifurcations of periodic orbits that wind around the cylinder.

The bifurcation diagram for case D was numerically verified for $a = -1$, $c = 2$, $s = -1$, as is shown in figure 15. The overview in panel (a) shows that the complicated bifurcation structure we just described indeed occurs quite close to the SNP point $D-$. When zooming in near Δ in panel (b) one distinguishes the curves T and T_2 of the

Table 1. Numerical parameter values used for the phase portraits of system (3); $a = -1$ and $s = -1$ are fixed.

orbit	ν_1	ν_2	c
Δ	0.249881	-1.89054	2.0
R	0.202939	-1.9058	2.0
L	0.270109	-1.88371	2.0
J	0.804746	-1.40699	0.0
W	0.26	-1.96664	2
$\overline{W}$	0.75	-1.44885	0.0
T	0.180434	-1.86617	2.0
T_2	0.2462469	-1.937119	2.0
T_3	0.261015	-1.96863	2.0
U	0.187843	-1.91016	2.0
U_2	0.117017	-1.93419	2.0
U_3	0.119672	-1.93429	2.0
3	0.75	-1.44	0.0
20	0.75	-1.44885	0.0
21	0.75	-1.45	0.0
18	0.75	-1.458	0.0

sequence T_i accumulating on W. To see the accumulation of the U_i we need to zoom in even further in panel (c), where the curves U, U_2 and U_3 can be seen accumulating on the curve SL. Notice further that the curves T_i and W approach Δ along the direction of R. Finally, the enlargement in panel (d) shows the curve SL connecting H and L, which is numerical evidence that the triangle Δ is unfolded generically in (3).

Figure 16 shows AUTO data of homoclinic and heteroclinic orbits along global bifurcation curves as the organizing center Δ is approached; the orbit corresponding to the respective endpoint of the curve approximately at Δ is shown boldfaced. It can be seen very clearly how the homoclinic orbit R approaches the extra saddle, while the homoclinic loop L approaches the triangle Δ by getting closer and closer to the relevant section of the invariant circle. The curves T and U each consist of one codimension-one part of Δ, and they cross each other at the organising center. The next orbits T_2 and U_2 in the sequence are shown in the covering space. The convergence to Δ is less pronounced for T_2 than it is for U_2. In fact, the numerics become increasingly difficult as one gets closer to triangle. Finally, W and SL are also shown to approach Δ in the covering space.

The transition from case A to case D, when the parameter c is increased, involves quite a number of codimension-three bifurcations. The exact nature and order of these bifurcation is beyond the scope of this paper.

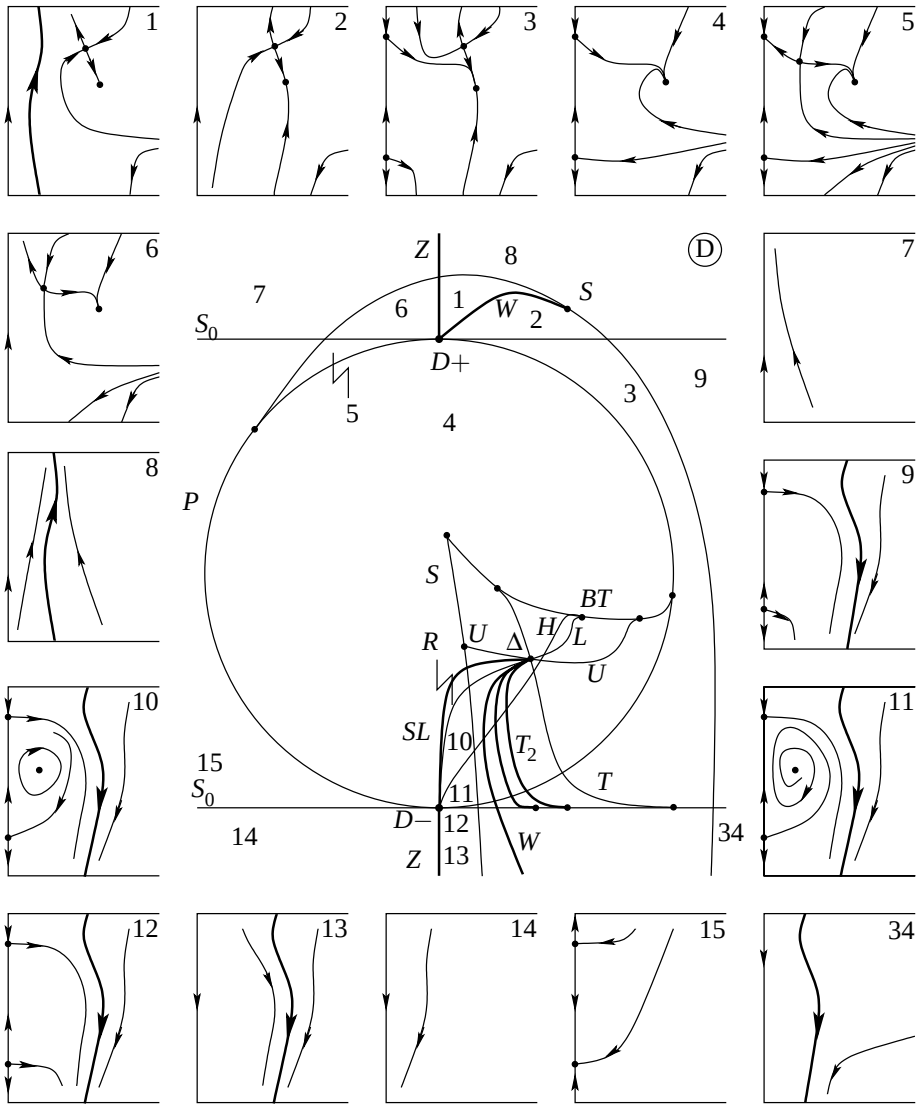

Figure 13. Qualitative bifurcation diagram for case D.

4. Semiconductor laser with optical injection

We considered case D as one of three cases of incomplete unfoldings in [19] because it appears in the model of a semiconductor laser subject to optical injection that motivated this study.

A semiconductor laser receiving optically injected light of a second laser of strength κ and frequency ω is a classic laser system. The idea was originally to improve the optical qualities of the laser, such as its line width, by having it lock to the external light. For suitable values of κ and ω this can indeed be achieved, but it turned out that this laser system can display an astonishing array of dynamics, including quasiperiodic and chaotic dynamics; see [29, 30, 32] as entry points to the literature.

A single-mode semiconductor laser with injection is well described by a three-

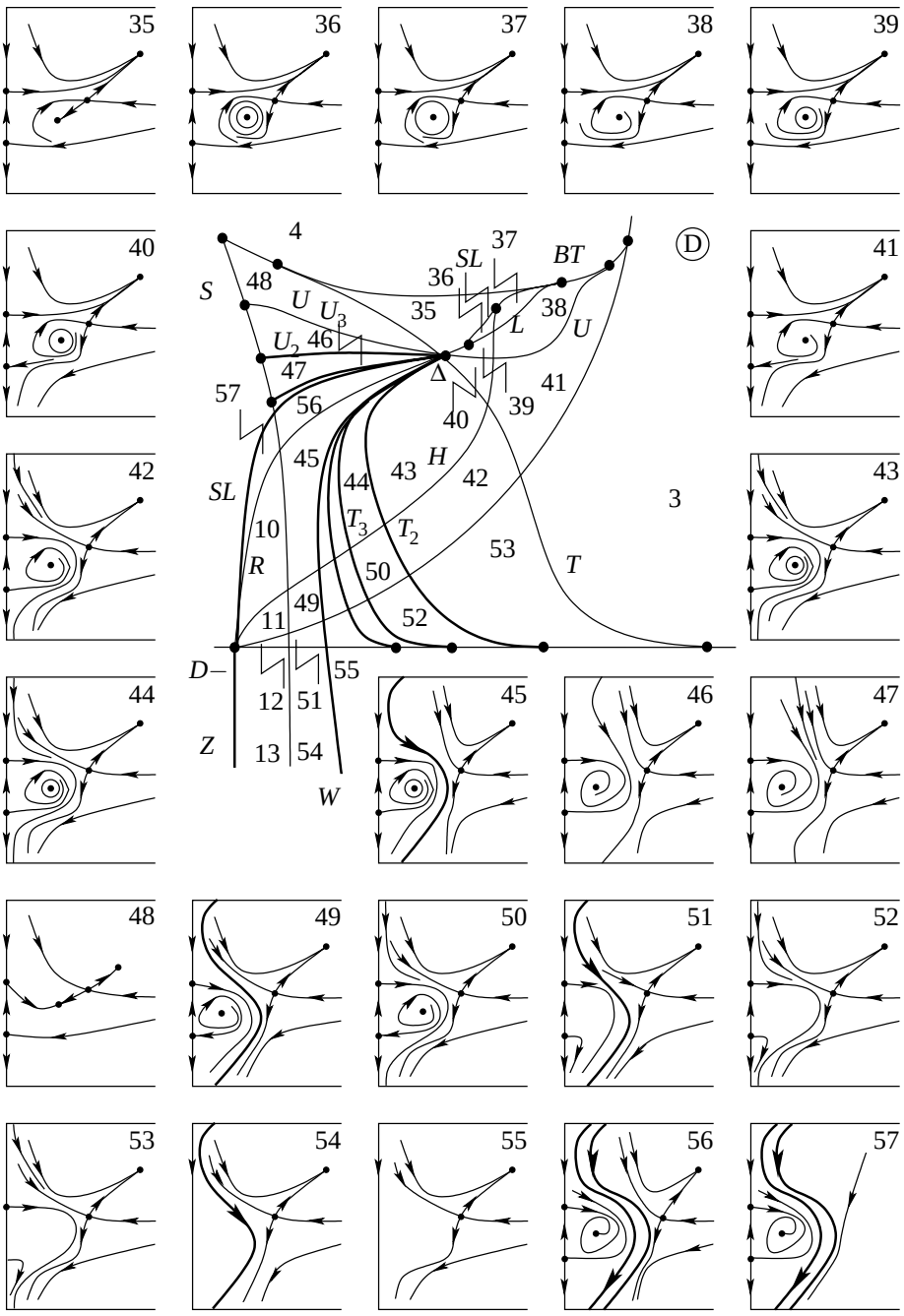

Figure 14. Enlargement of the qualitative bifurcation diagram for case D.

dimensional system of ordinary differential equations, called the rate equations, which can be written as

$$\dot{E} = \frac{1}{2}\xi(1+i\alpha)nE + \kappa e^{i\omega t} \tag{18}$$

$$\dot{n} = -2\lambda_R n - (\Gamma_0 + \xi n)(|E|^2 - P_0). \tag{19}$$

Here E is the complex electric field and n denotes the inversion (the number of electron-hole pairs inside the laser). The parameters α, ξ, λ_R and Γ_0 describe material properties

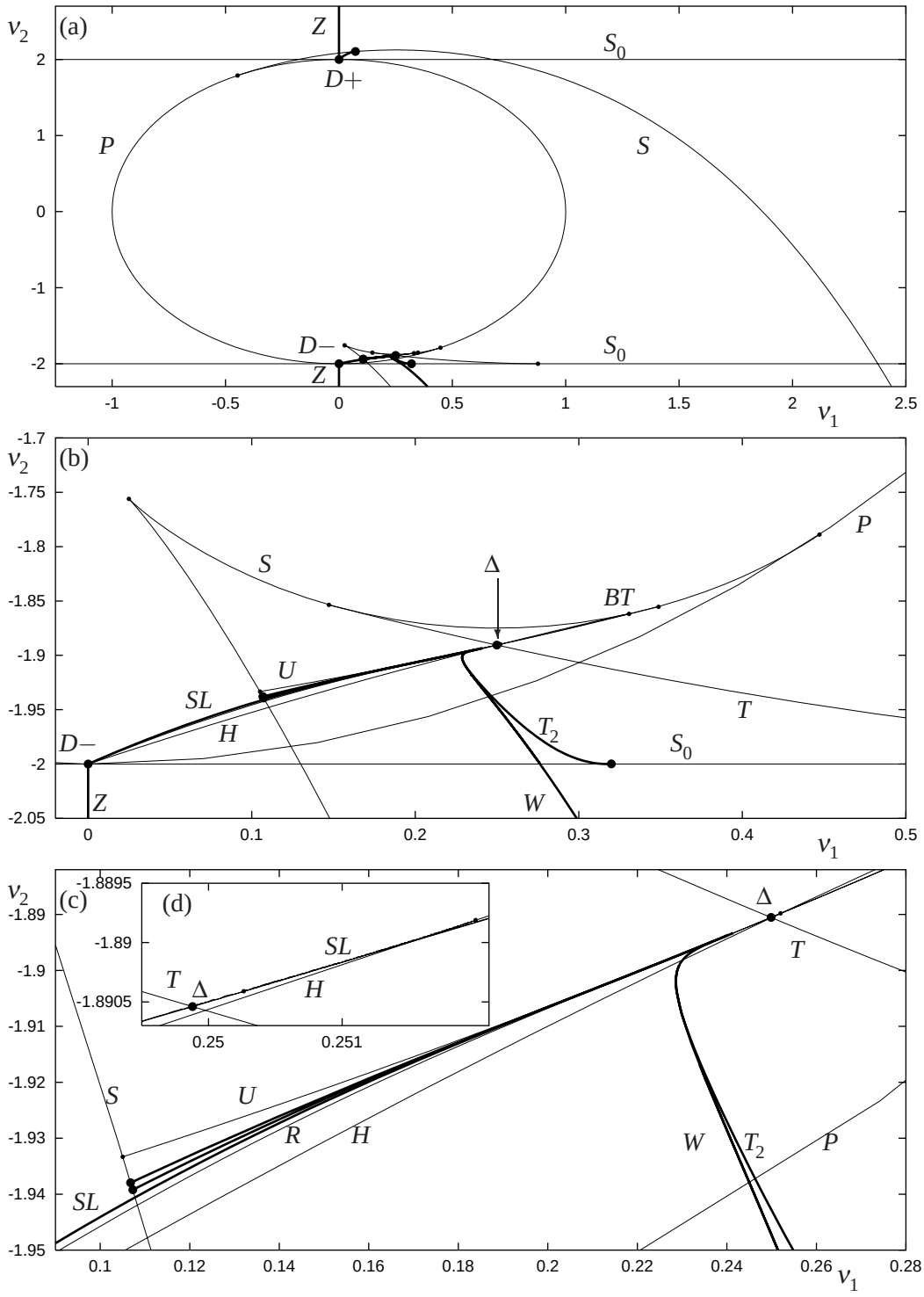

Figure 15. Numerical overview of case D (a) and successive enlargements of the neighbourhood of $D-$ (b) and near the triangle (c)–(d). Here $s = -1$, $a = -1$ and $c = 2$.

of the laser, and P_0 is the pump current; see [21, 32] for details.

System (19) has a SNP point G that acts as an organising center of the dynamics.

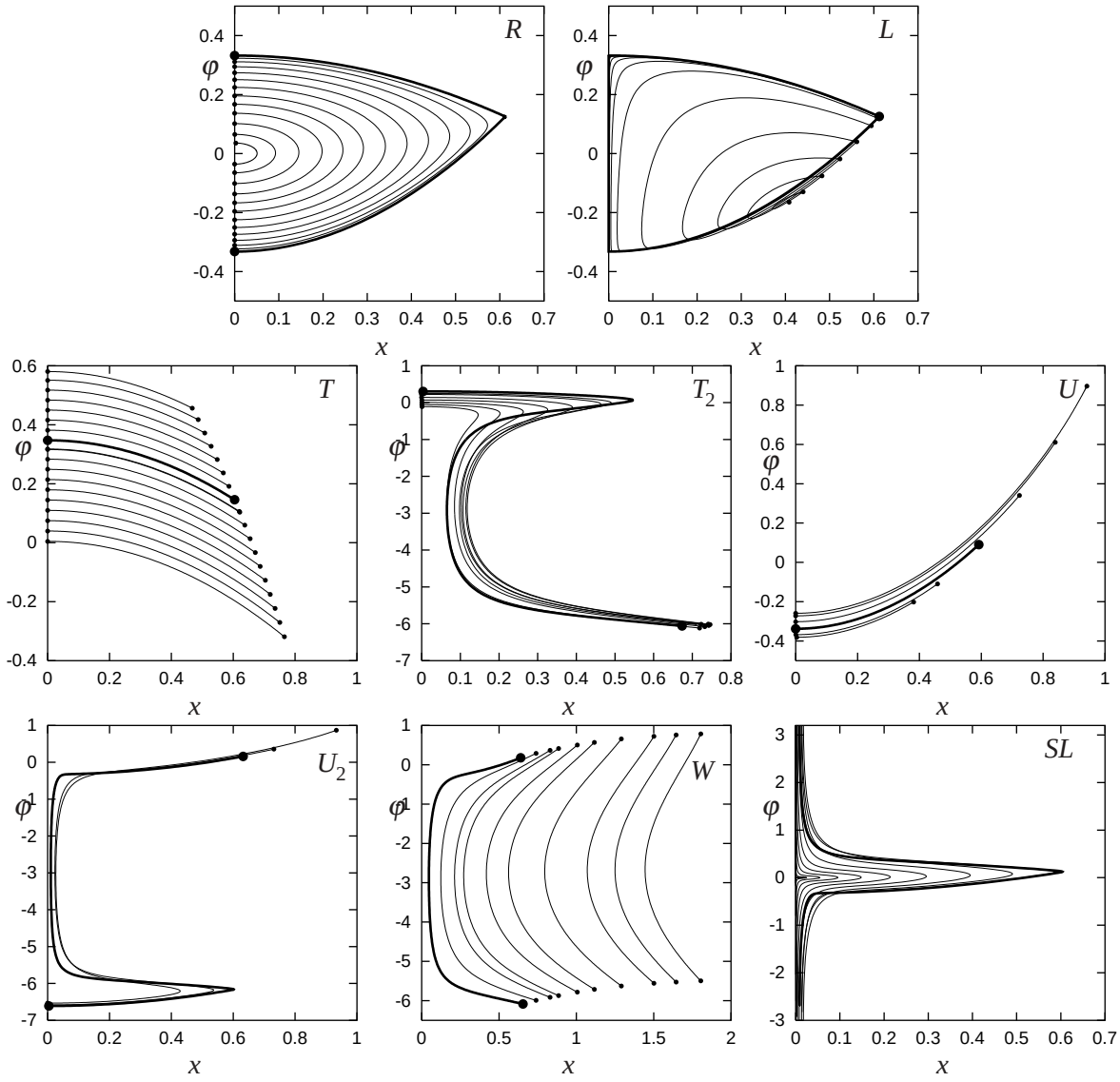

Figure 16. Phase portraits of orbits as they are continued along the respective bifurcation curves in Figure 15. Here $s = -1$, $a = -1$ and $c = 2$.

In [9] equations (19) were reduced to a two-dimensional vector field involving Bessel functions by averaging over an intrinsic oscillation of diode lasers (the so-called relaxation oscillation). To perform a bifurcation analysis near the point G this vector field was Taylor expanded and truncated at third order of the amplitude term in [32], yielding the reduced system

$$\dot{\rho} = -\left[\Gamma - \frac{1}{2}K\sin(\varphi + A_\alpha)\right]\rho - \left[\frac{B}{2(1+\alpha^2)} - \frac{K}{16}\sin(\varphi + 2A_\alpha)\right]\rho^3 \quad (20)$$

$$\dot{\varphi} = (\omega - K\cos\varphi) - \frac{1}{4}K\cos(\varphi + A_\alpha)\rho^2. \quad (21)$$

The variable ρ is a measure of the amplitude of the relaxation oscillation, and φ is the angular component of the electric field. Further, K is the rescaled injection strength,

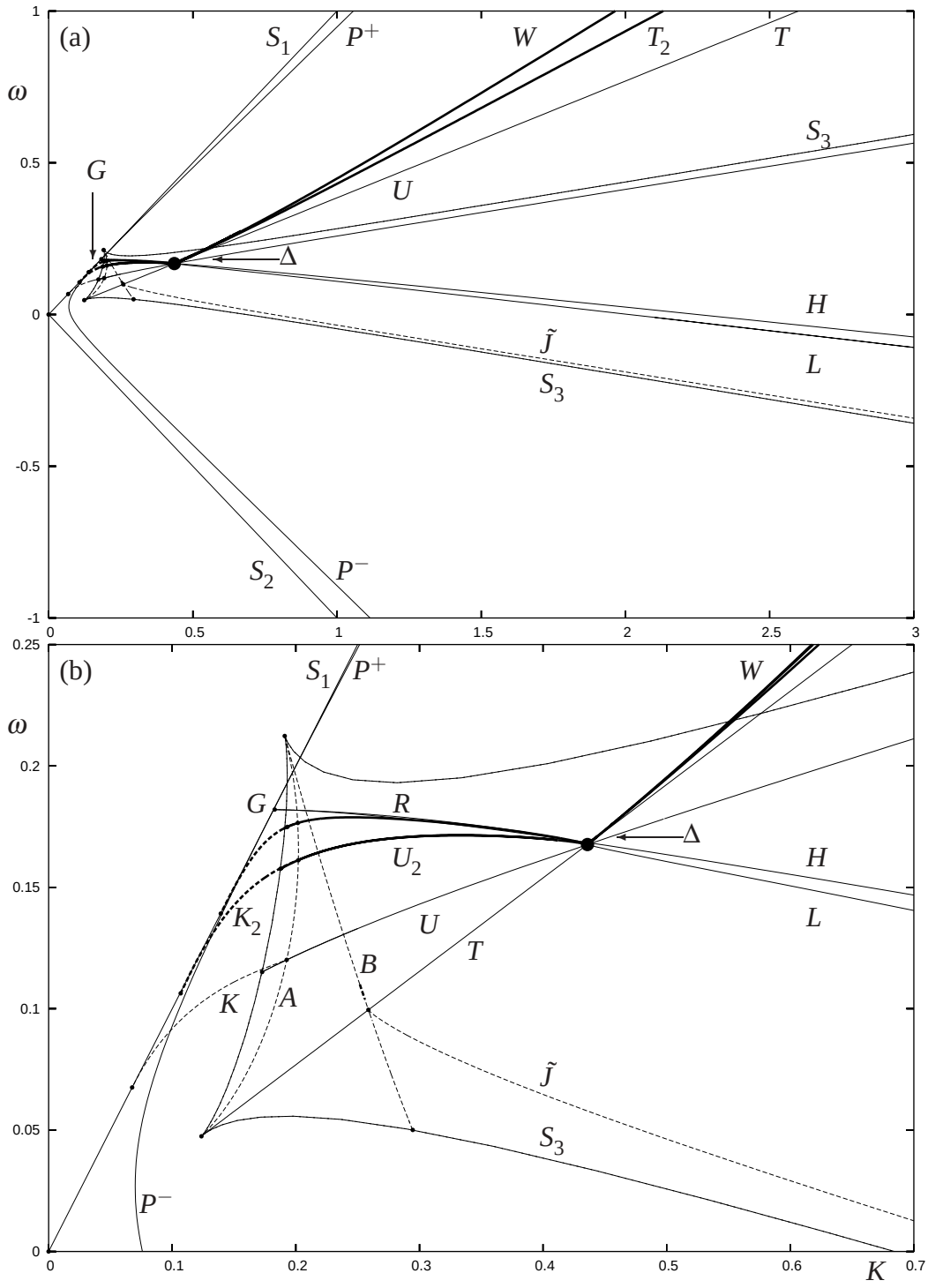

Figure 17. The bifurcation diagram of (21) in the the (K, ω)-plane (a) and two successive enlargements (b)–(c). Here $\alpha = 5.0$, $\Gamma = 0.035$, and $B = 0.015$; for all other parameter values see table 2.

ω is measured relative to the frequency of the free running laser, and α, B and Γ are rescaled material constants of the laser.

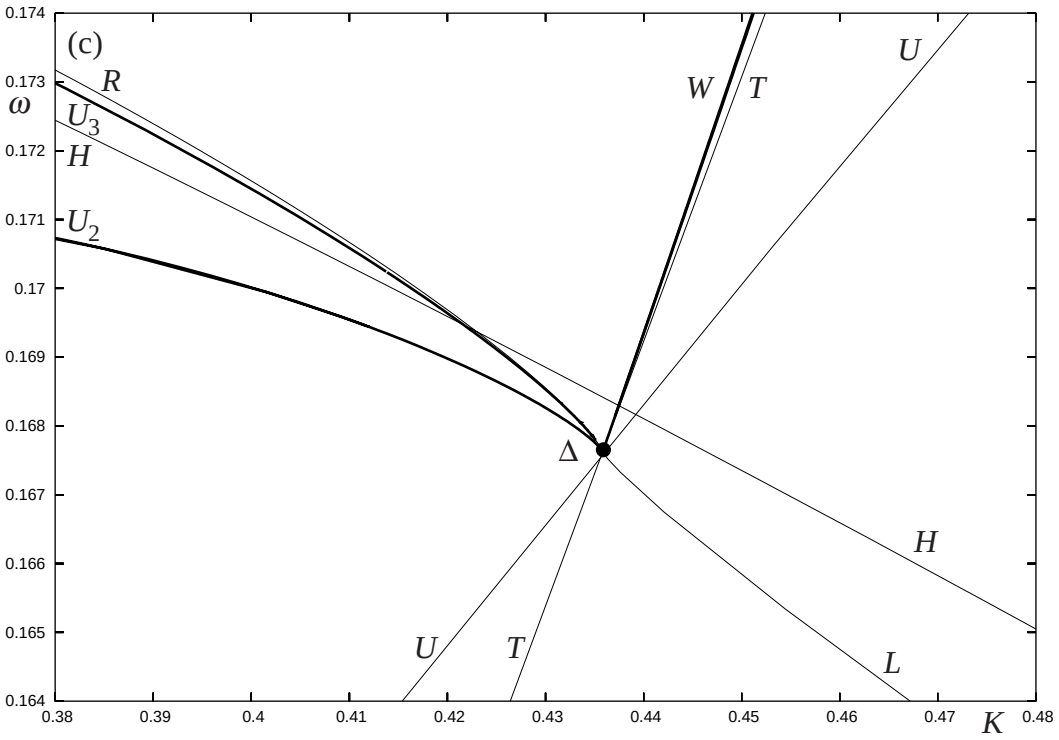

Figure 17 (continued).

System (21) is reflectionally symmetric in ρ and 2π-periodic in φ, so that it is a vector field on the half-cylinder $\mathbb{R}^+ \times S^1$, just like (3). It was already found in [32] that the heteroclinic bifurcation R (in our notation) leads to a large periodic orbit winding around the cylinder. Physically, an excursion around the cylinder corresponds to a 2π phase shift of the phase difference between the laser and the injected light; see also [20, 28, 32, 34].

We present in figure 17 bifurcation diagrams in the (K, ω)-plane of (21) for realistic values of the laser parameters, namely $\alpha = 5.0$, $B = 0.015$ and $\Gamma = 0.035$. These results were obtained by Cathryn Crooks in [8] during a systematic exploration of the effect of the global reinjection. Curves that are plotted normally again correspond to bifurcations that are already present in a neighbourhood of the SNP point without reinjection, while boldfaced curves denote bifurcations that are due to global reinjection. It turns out that in system (21) we find an additional saddle point, not present in model (3). This results in extra bifurcations that are denoted in Figures 17 by dashed curves and explained below.

While it is not possible to bring system (21) into the form of (3), the overview in figure 17 (a) shows that there are two main organizing centers, the SNP bifurcation G and the triangle Δ of heteroclinic orbits, just as it is the case near the SNP point $D-$ in figure 16. The enlargement in figure 17 (b) should be compared with that in figure 16 (b). Finally, figure 17 (c) is a close-up near Δ, clearly showing the homoclinic curves U_2 and U_3 near R and the curve T near W. Notice that the Hopf bifurcation

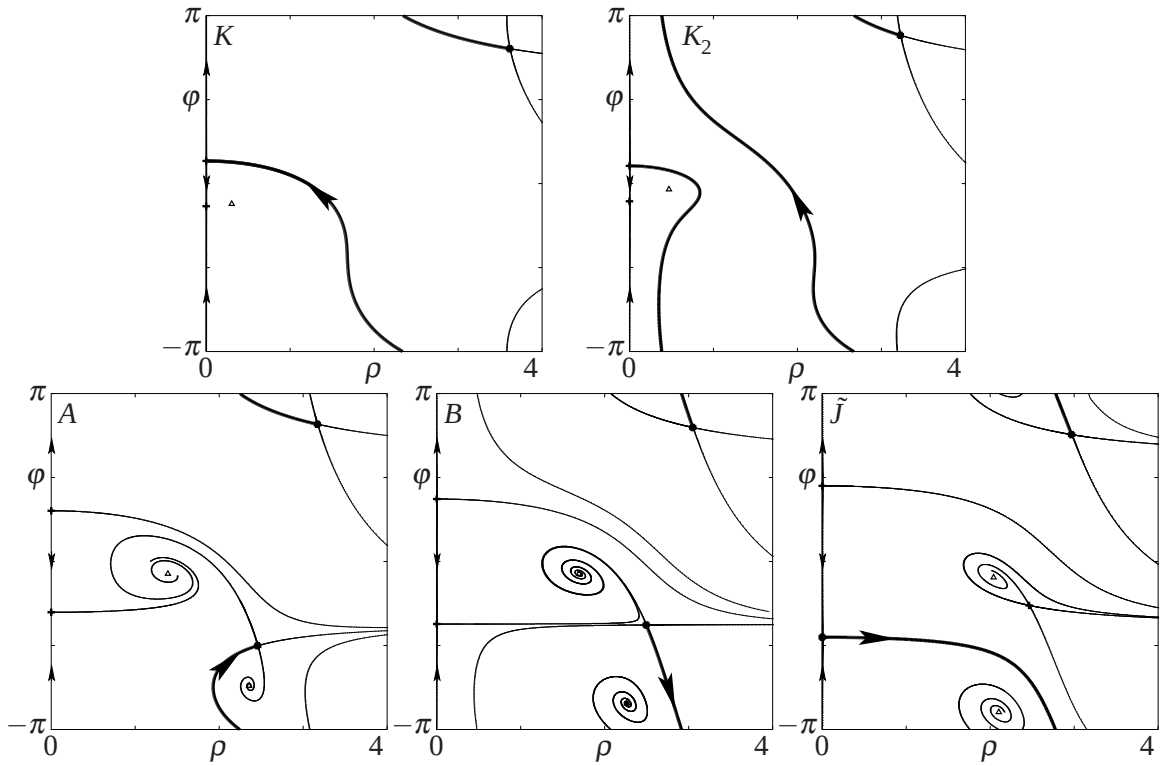

Figure 18. Numerical phase portraits of the extra heteroclinic orbits that are involved in the laser model. The parameters $\alpha = 5$, $\Gamma = 0.035$, and $B = 0.015$ are the same for all phase portraits. The respective values of the parameters K and ω are in table 2.

curve H misses Δ, which is the generic case.

Overall, this numerical study shows that the presence of a SNP bifurcation of type $D-$, as was shown in [32], combined with global reinjection explains the complicated dynamics found in the laser model (21). This shows that model (3) is indeed a good global model (a bit like a normal form) — it captures the key dynamics in an easy model in a neighbourhood of the SNH point and the reinjection loop.

Note that the extra bifurcations due to the reinjection mechanism are important from the physical point of view, because a global excursion corresponds to a 2π phase slip of the frequency of the laser with respect to the frequency of the injected light [32].

However, there are bifurcations present in figure 17 (b) that do not occur in the model (21). The dashed curves are due to the presence in the laser model of a further saddle point off the invariant axis. Figures 18 shows that the extra heteroclinic bifurcations A, B, $\tilde{J}$ and K_i may appear as a consequence. In particular, when U_i crosses

Table 2. Numerical parameter values used for the phase portraits of the laser system; $\alpha = 5$, $\Gamma = 0.035$, and $B = 0.015$ were fixed.

orbit	K	ω
K	0.1016135	0.09265677
K_2	0.152121	0.1438588
A	0.187383	0.1090994
B	0.2578078	0.100872
$\tilde{J}$	0.4082675	0.06310408

the curve A, the two heteroclinic orbits form a codimension-two heteroclinic connection that also has the curve K_i as its limit. This bifurcation can be seen as gluing U_i to A to obtain K_i, which then misses the middle saddle point. The curves K_i extend beyond the saddle-node bifurcation curve S_3 and end on S_1 when the saddle on the invariant circle disappears. The end points of K_i appear to accumulate on G; see figure 17.

To include this extra saddle point and the associated bifurcations in a vector field model one will have to go up to higher order in x in (3). What the appropriate higher order trigonometric terms in φ would be is an open question.

5. Discussion

In this paper we showed that the existence of a global reinjection mechanism gives rise to many interesting bifurcations. We considered a planar model vector field and studied its global bifurcation structure. The most complicated case of an SNP point was found to organize the dynamics of a laser subject to optical injection.

In this paper we considered the planar vector field approximation near a saddle-node Hopf bifurcation, by studying a saddle-node pitchfork bifurcation, as is common in the field. To translate back to the dynamics near an SNH point in a full three-dimensional vector field, one needs to suspend a small perturbation of the planar normal form. This is a standard procedure to get from averaged equations back to the original problem, and it is explained in quite some detail in [23, Chapter 8.5] for the case of the SNH bifurcation. General theory states that curves of homoclinic and heteroclinic bifurcations 'open up' to horns of homoclinic intersections, bounded by curves of homoclinic tangencies. These new boundary curves have exponential contact at the respective codimension-two singularities. What is more, the invariant circle $\{x = 0\}$ is not preserved. In the presence of global reinjection, this leads to the possibility of periodic and homoclinic orbits that stay in a neighbourhood of the bifurcating equilibria for a while and then make global excursions away and back to that neighbourhood. Such orbits were indeed found in the injection laser; see, for example, [20, 22, 32, 34].

It is an interesting topic for future research to unravel the exact bifurcation structure of these periodic and homoclinic orbits. A first exploration of the full three-dimensional rate equations of the injection laser (see [32] for the exact equations) indicates that one

can find periodic orbits that make any combination of internal and external loops; see also [22].

Finally, we remark that it is an interesting topic for future research to study the influence of a global reinjection mechanism on other (codimension-two) local bifurcations. The approach taken here of constructing a global vector field model should prove to be useful in situations where the local bifurcation can be thought of as taking place on an invariant circle.

Acknowledgments

We are grateful to Cathryn Crooks for providing the original data of the bifurcation diagrams presented in figure 17, and to Alan Champneys, Henk Broer and Renato Vitolo for helpful discussions. The research of B.K. was supported by an EPSRC Advanced Fellowship grant and that of B.O. by EPSRC grant GR/R23695/01.

References

[1] Back A, Guckenheimer J, Myers M, Wicklin F and Worfolk P 1992 DsTool: Computer assisted exploration of dynamical systems *Notices AMS* **39**(4), 303–309.

[2] Broer H W and Vegter G 1992 Bifurcational aspects of parametric resonance *in* Dynamics Reported, New Series Vol. 1 Springer-Verlag pp. 1–51.

[3] Champneys A R and Kirk V 2003 The entwined wiggling of homoclinic curves emerging from saddle-node/Hopf instabilities *Appl. Nonl. Math. Preprint* **2003.18**, University of Bristol. `http://www.enm.bris.ac.uk/anm/preprints/2003r18.html`.

[4] Champneys A R and Kuznetsov Y A 1994 Numerical detection and continuation of codimension-two homoclinic bifurcations *Int. J. Bifurcation and Chaos* **4**(4), 785–822.

[5] Champneys A R, Kuznetsov Y A and Sandstede B 1996 A numerical toolbox for homoclinic bifurcation analysis *Int. J. Bifurcation and Chaos* **6**(5), 867–887.

[6] Chow S N, Deng B and Fiedler B 1990 Homoclinic bifurcation at resonant eigenvalues *J. Dyn. Diff. Eqns.* **2**(2), 177–244.

[7] Chow S N, Li C and Wang D 1994 *Normal Forms and Bifurcation of Planar Vector Fields* Cambridge University Press.

[8] Crooks C 2000 Nonlinear dynamics of an optically injected diode laser Master's thesis University of Bristol.

[9] de Jagher P C, van der Graaf W A and Lenstra D 1996 Relaxation-oscillation phenomena in an injection locked semiconductor laser *Quant. Semiclass. Opt.* **8**, 805–822.

[10] Doedel E J, Paffenroth R C, Champneys A R, Fairgrieve T F, Kuznetsov Y A, Sandstede B and Wang X 2001 *AUTO 2000: Continuation and Bifurcation Software for Ordinary Differential Equations (with HomCont).* `http://sourceforge.net/projects/auto2000/`.

[11] Gaspard, P 1993 Local birth of homoclinic chaos em Phys. D **62**1-4), 94–122.

[12] Gavrilov N K 1978 On some bifurcations of equilibria with a zero and a pair of purely imaginary eigenvalues *in* E. A Leontovich-Adronova, ed. *Methods of the Qualitative Theory of Differential Equations* Gor'kov Gos. Univ. Gorr'kij pp. 33–40. in Russian.

[13] Gavrilov N K 1985 On some bifurcations of equilibria of codimension two of divergence-free vector fields *in* Methods of the Qualitative Theory of Differential Equations Gor'kov Gos. Univ. Gorr'kij pp. 46–55. in Russian.

[14] Gavrilov N K 1987 On bifurcations of equilibria with a zero and a pair of purely imaginary

eigenvalues with an additional degeneracy *in* Methods of the Qualitative Theory of Differential Equations Gor'kov Gos. Univ. Gorr'kij pp. 43–51. in Russian.

[15] Guckenheimer J 1981 On a codimension two bifurcation *in* D. A Rand and L. S Young, eds *Dynamical Systems and Turbulence* Vol. 998 of *Springer Lecture Notes in Mathematics* Springer-Verlag, Berlin pp. 99–142.

[16] Guckenheimer J and Holmes P 1983 *Nonlinear Oscillations, Dynamical Systems and Bifurcations of Vector Fields* Springer.

[17] Kirk V 1991 Breaking of symmetry in the saddle-node Hopf bifurcation *Phys. Lett. A* **154**, 243–248.

[18] Knobloch E and Moore D 1990 Minimal model of binary fluid convection *Physical Review A* **42**(8), 4693–4709.

[19] Krauskopf B and Rousseau C 1997 Codimension-three unfoldings of reflectionally symmetric planar vector fields *Nonlinearity* **10**(5), 1115–1150.

[20] Krauskopf B, Tollenaar N and Lenstra D 1998 Tori and their bifurcations in an optically injected semiconductor laser *Optics Communications* **156**(1–3), 158–169.

[21] Krauskopf B, van der Graaf W A and Lenstra D 1997 Bifurcations of relaxation oscillations in an optically injected diode laser *Quantum Semiclass. Opt.* **9**, 797–809.

[22] Krauskopf B and Wieczorek S M 2002 Accumulating regions of winding periodic orbits in optically driven lasers *Physica D* **173**, 97–113.

[23] Kuznetsov Y A 1998 *Elements of Applied Bifurcation Theory* 2nd edn Springer.

[24] Moroz I 1990 Multiple instabilities in rotating convection *Geophys. Astrophys. Fluid Dynamics* **53**, 183–204.

[25] Mullin T, Tavener S J and Cliffe K A 1989 An experimental and numerical study of a codimension-2 bifurcation in a rotating annulus *Europhysics Letters* **8**(3), 251–256.

[26] Shilnikov A, Nicolis G and Nicolis C 1995 Bifurcation and predictability analysis of a low-order atmospheric circulation mode *Int. Journal of Bifurcation and Chaos* **5**, 1701–1711.

[27] Sneyd J, LeBeau A and Yule D 2000 Travelling waves of calcium in pancreatic acinar cells: model construction and bifurcation analysis *Physica D* **145**, 158–179.

[28] Solari H G and Oppo G L 1994 Laser with injected signal: Perturbation of an invariant circle *Optical Communications* **111**, 173–190.

[29] Tartwijk G H M V and Agrawal G P 1998 Laser instabilities: a modern perspective *Prog. Quantum Electron.* **22**, 43–122.

[30] van Tartwijk G H M and Lenstra D 1995 Semiconductor lasers with optical injection and feedback *Quant. Semiclass. Opt.* **7**, 87–143.

[31] Vitolo R 2003 Bifurcations of attractors in 3D diffeomorphisms: a study in experimental mathematics. PhD Thesis. University of Groningen. to appear.

[32] Wieczorek S M, Krauskopf B and Lenstra D 1999 A unifying view of bifurcations in a semiconductor laser subject to optical injection *Optics Communications* **172**(1–6), 279–295.

[33] Yeung M K S and Strogatz S H 1998 Nonlinear dynamics of a solid-state laser with injection *Phys. Rev. E* **58**(4), 4421–4435.

[34] Zimmermann M, Natiello M and Solari H 1997 Shil'nikov-saddle-node interaction near a codimension 2 bifurcation: Laser with injected signal *Physica D* **109**, 293–314.